Article

Thermal Conductivity in Aged Li-Ion Cells under Various Compression Conditions and State-of-Charge

Georgi Kovachev [1,*] **, Andrea Astner** [1] **, Gregor Gstrein** [1] **, Luigi Aiello** [1] **, Johann Hemmer** [2] **, Wolfgang Sinz** [1] **and Christian Ellersdorfer** [1]

1   Vehicle Safety Institute, Graz University of Technology, Inffeldgasse 23/I, 8010 Graz, Austria; andrea.astner@student.tugraz.at (A.A.); gregor.gstrein@tugraz.at (G.G.); luigi.aiello@tugraz.at (L.A.); wolfgang.sinz@tugraz.at (W.S.); christian.ellersdorfer@tugraz.at (C.E.)
2   MUP Technologies GmbH, Innovationspark 3, 8152 Stallhofen, Austria; hemmer.johann@sfl-technologies.com
*   Correspondence: georgi.kovachev@tugraz.at; Tel.: +43-(0)-316-873-303-66

Abstract: Thermal conductivity (TC) is a parameter, which significantly influences the spatial temperature gradients of lithium ion batteries in operative or abuse conditions. It affects the dissipation of the generated heat by the cell during normal operation or during thermal runaway propagation from one cell to the next after an external short circuit. Hence, the thermal conductivity is a parameter of great importance, which concurs to assess the safety of a Li-ion battery. In this work, an already validated, non-destructive measurement procedure was adopted for the determination of the evolution of the through-plane thermal conductivity of 41 Ah commercially available Li-ion pouch cells ($LiNiMnCoO_2$-$LiMn_2O_4$/Graphite) as function of battery lifetime and state of charge (SOC). Results show a negative parabolic behaviour of the thermal conductivity over the battery SOC-range. In addition, an average decrease of TC in thickness direction of around 4% and 23% was measured for cells cycled at 60 °C with and without compression, respectively. It was shown that pretension force during cycling reduces battery degradation and thus minimises the effect of ageing on the thermal parameter deterioration. Nevertheless, this study highlights the need of adjustment of the battery pack cooling system due to the deterioration of thermal conductivity after certain battery lifetime with the aim of reducing the risk of battery overheating after certain product life.

Keywords: through-plane thermal conductivity; aged Li-ion batteries; safety of electric vehicles

1. Introduction

In last decade, environmental aspects including reduction of greenhouse gases emissions, low carbon footprint and high-energy efficiency have become important issues, hence electric and hybrid electric vehicles (EV and HEV) represent a green alternative for use in transportation instead of internal combustion engine vehicles. As energy storage system and power source for this vehicles, lithium ion secondary batteries (LIBs) are considered as most promising, due to their outstanding properties such as high energy density as well as long cycle life [1–3]. Higher energy density also means higher heat losses, which increase the temperature rise during cell operation possibly leading to thermal runaway [4]. Once the thermal runaway is triggered within a single cell, the heat transfer can cause cell-to-cell thermal runaway propagation and thus catastrophic hazards [5]. Several fire accidents associated with thermal runaway occurred and made people aware of thermal safety of Li-ion cells [2]. Thermal properties such as the thermal conductivity dramatically influence the highest temperature that a cell can safely withstand as well as the thermal runaway propagation [4,5]. Therefore, research on thermal conductivity of LIBs is fundamental to prevent the similar occurrence of fire accidents.

Significant amount of research on thermal conductivity was accomplished on component level for wet and dry sample materials [1,6–8], where a value of the total TC of the cell can be estimated based on knowledge of the internal structure of the battery. However,

this method allows the determination of the TC value for each battery layer, but it hardly represents the real case of a closed battery system and makes the evaluation of the influence of SOC difficult due to its destructive nature.

Several studies focused on analysis of the full cell using different measurement approaches. Arzberger et al. [9] investigated the thermal conductivity change for three different temperatures of a self-constructed pouch cell at 50% SOC. Drake et al. [10] adopted a non-destructive procedure to determine the average thermal conductivity of 26650 and 18650 cylindrical LiFePO$_4$ (LFP) cells. Steinhardt et al. [11] explored the dependency of thermal conductivity on temperature and applied compression force of NMC-111 prismatic batteries. These studies, however, did not show the behavior of thermal conductivity over the battery SOC-range or after battery ageing.

State of charge dependency was investigated in literature; the results of the according studies, however, show contradicting trends for the thermal conductivity. Sheng et al. [2] and Bazinski et al. [12] indicated an increase in the thermal parameter value with decreasing SOC. Other researchers measured a parabolic behavior of TC with state of charge for LFP [3,13] and lithium-titanate-oxide (LTO) [4] cells, indicating a peak value in the range of 50–70% SOC. None of these investigations focused on evaluating if and how this relationship changes with cycle life.

Maleki et al. [14] and Richter et al. [1] explored the effect of the ageing process on the thermal conductivity, however this investigation was carried out on single electrodes. Vertiz et al. [3] measured a decrease of 29% of the TC in a degraded cell with 80% residual capacity, however no additional information was given how the cell was aged and no explanation for the occurred difference was found.

Generally, there is only little data available in literature on how cycle ageing affects the thermal conductivity of the battery over the whole SOC-range and no clear connection was made between cycling conditions, cell degradation and its thermal properties. It is well known, however, that during charge-discharge cycling side reactions occur between the electrodes and the electrolyte [15,16]. These effects lead to the formation and growth of a solid electrolyte interphase (SEI) film on the anode, loss of active material in the cathode and gas evolution. These processes are also accompanied by the consumption of the electrolyte solution. Such effects, which alter the internal structure of the cell, could significantly influence the cells transversal TC.

The main purpose of this work is to clarify the relationship between state of health (SOH), SOC and thermal conductivity of the investigated battery. For this reason, non-destructive measurements were conducted on fresh and cycle-aged cells in thickness direction for several different SOC. Possible reasons are highlighted, which could be the cause for the occurred changes in thermal conductivity. In addition, an assessment is made regarding the influence of cell compression during ageing on the change of the thermal conductivity. A recommendation is given on changes that can be made during battery pack production and battery use, which can prevent hazardous outcomes due to cell overheating.

2. Results

2.1. Trough-Plane Thermal Conductivity as a Function of SOC

The through-plane thermal conductivity was determined for four different SOC levels on three fresh batteries. It was calculated from the steady state values of the temperature difference and heat flux in combination with the results of the thickness measurements (see Appendix A), conducted according to the method described in Section 4. Figure 1a provides additional information on the thickness change with battery SOC. Each point on the presented curves represents an arithmetic mean value of the thickness, measured at twelve different locations on the surface of each cell. The test data showed an overall thickness increase with state of charge, where a thickness difference of approx. 1% was determined between fully charged and fully discharged cells.
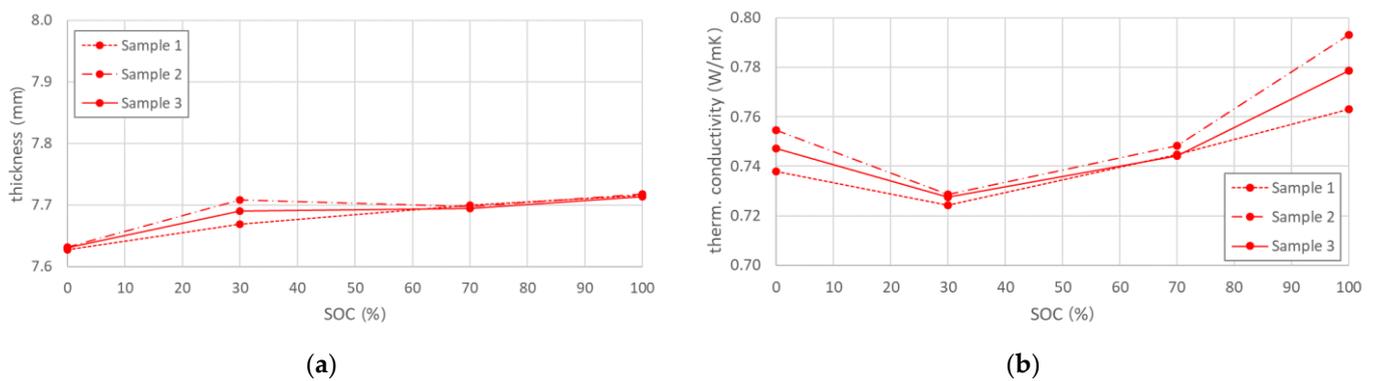
(a)

(b)

Figure 1. (**a**) Cell thickness variation over SOC for fresh cells (**b**) Calculated thermal conductivity of fresh cells, showing a negative parabolic behavior with SOC increase.

The evolution of the thermal conductivity as function of SOC is shown in Figure 1b. A negative parabolic dependence was observed for fresh cells, where highest values were measured for the fully charged state. The highest standard deviation of all samples from the average through-plane TC value was less than 2%, which indicates a good reproducibility of the tests but also a controlled manufacturing process of the analysed cells. A summary of the results with their respective deviations are summarised in Table 1.

Table 1. Results for the average cell thickness and average through-plane thermal conductivity for fresh cells in dependence with SOC.

SOC (%)	Average Thickness d (mm)	Average Through-Plane TC k (WK^{-1}m^{-1})
0	7.631 ± 0.0%	0.747 ± 1.2%
30	7.691 ± 0.3%	0.727 ± 0.4%
70	7.695 ± 0.1%	0.744 ± 0.6%
100	7.713 ± 0.1%	0.779 ± 2.0%

The thickness and thermal conductivity data, determined for fresh cells is used as reference for the differently aged batteries.

2.2. Thermal Conductivity of Aged Cells

In order to assess the influence of product life onto the thermal conductivity of LIBs, measurements were performed on differently aged cells. The respective ageing procedures are described in detail in Section 4. Results of the conducted tests can be seen in Figure 2. An overall thickness increase for aged cells over the whole SOC-range was determined (Figure 2a). A similar trend however was observed to that of fresh batteries, where a difference in thickness of about 1% was evaluated between fully charged and discharged cells. The total amount of irreversible swelling was shown to be also dependent on the compression force applied to the component stack during ageing. Cells, cycled without pretension, experienced a thickness increase slightly higher than 10%. For the typical pretension of 0.06 MPa, the value of total cell expansion was only about half as much. In the case of high pretension during cycling, the rise in cell thickness was determined to be in the order of 3%. The measured thickness values for each investigated SOC were used for the calculation of the thermal conductivity of aged batteries.
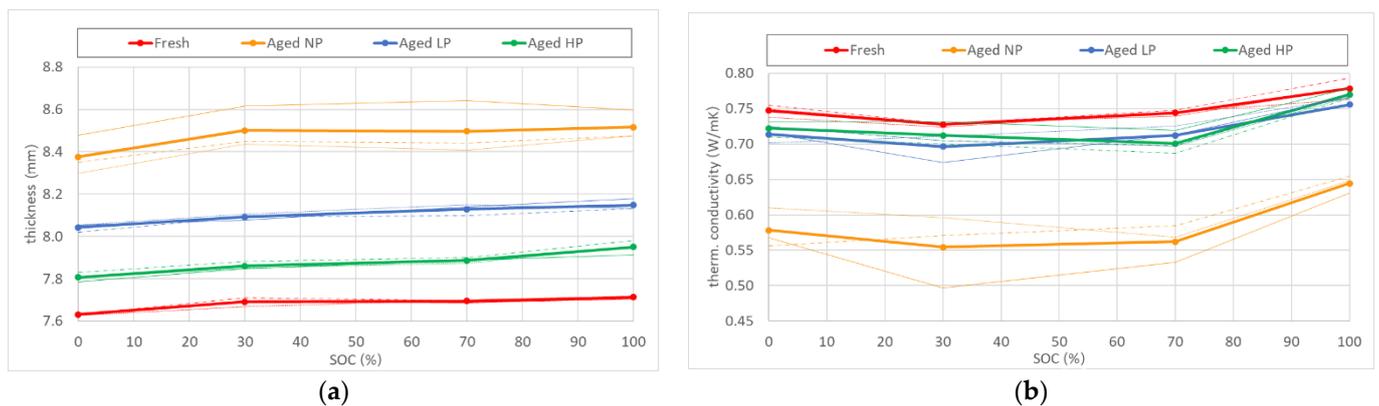
Figure 2. (**a**) Thickness increase with SOC for different aged cells (**b**) Influence of product life on the thermal conductivity of cells aged under different compression forces.

The negative parabolic dependency of TC on SOC was again observed for every type of aged cell. Overall, thermal conductivity decreased with aging (Figure 2b). The degree of deterioration strongly varied with the level of compression force, applied on the battery during cycling. In the case of no pretension (NP), TC experienced a reduction of 23%, whereas for the realistic use case (LP) the decrease was measured to be six times less. The result for the thermal conductivity of cells, aged with a strong compression acting on the component stack (HP), were similar to the case of LP-aged cells. Measurements of through-plane TC showed a decrease of ~4% from the nominal value, measured for fresh cells. A summary of the test results can be found in Table 2.

Table 2. Average thickness and average through-plane thermal conductivity values for fresh and aged cells.

	Average Thickness d (mm)				Average Through-Plane TC k (WK^{-1}m^{-1})			
Ageing type	0% SOC	30% SOC	70% SOC	100% SOC	0% SOC	30% SOC	70% SOC	100% SOC
Fresh	7.63 ± 0.0%	7.69 ± 0.3%	7.70 ± 0.1%	7.71 ± 0.1%	0.75 ± 1.2%	0.73 ± 0.4%	0.74 ± 0.6%	0.80 ± 2.0%
NP	8.38 ± 9.76%	8.49 ± 10.53%	8.50 ± 10.41%	8.52 ± 10.41%	0.58 ± 22.6%	0.55 ± 23.8%	0.56 ± 24.5%	0.65 ± 17.2%
LP	8.04 ± 5.39%	8.09 ± 5.22%	8.13 ± 5.64%	8.015 ± 5.63%	0.71 ± 4.4%	0.69 ± 4.3%	0.71 ± 4.3%	0.77 ± 2.9%
HP	7.81 ± 2.31%	7.86 ± 2.21%	7.89 ± 2.50%	7.95 ± 3.06%	0.72 ± 3.3%	0.71 ± 2.1%	0.70 ± 5.8%	0.77 ± 1.1%

3. Discussion

3.1. Influence of State-of-Charge on Thermal Conductivity

Through-plane thermal conductivity measurements revealed a minor negative parabolic dependency with increasing state of charge of the battery. In general, an average decrease of about 3–6% in TC is measured until the first 30% SOC are reached, after which it increases by 5–12% as the cells are charged to 100% SOC. The state of charge dependency can be simply addressed to the distribution and densities of Li-ions in the electrodes at different SOC. During different stages of lithiation/delithiation, the battery cathode active material (NMC) experiences structural changes which are related to phase transformations of the material [17]. These occur due to sudden changes of lithium ion/vacancy distribution at critical SOC-values, which would most likely affect the overall TC of the cell. Thermal conductivity in thickness direction of layered graphite compounds also shows a negative parabolic behaviour during different stages of lithiation [18]. TC of pure graphite reduces as lithium ions occupy vacancies in the lattice structure of the material in the initial stage. If further lithiated, the thermal conductivity of the negative electrode increases until reaching a fully charged state.

3.2. Influence of Cycle Life on Thermal Conductivity

During cycling of LIB the internal structure of the components changes and the capacity drops [15,16]. The reason for this is, amongst others, the consumption of lithium ions due to chemical reactions with the electrolyte and the subsequent formation and growth of the SEI layer at the battery anode. This process results in less lithium molecules

available for the charging-discharging process causing a capacity fade. The cells analysed show a loss of ~15% (HP, LP) and ~20% (NP) of their nominal capacity (Section 4), which indicates already a significant change compared to the fresh reference cell.

Degradation of the thermal conductivity over the whole SOC-range of aged cells was also seen, which can be correlated to the observed capacity degradation and to the underlying degradation mechanisms. The overall reduction of TC for each measured state of charge can be related to several different effects, the first of which is the consumption of active lithium for the growth of the SEI layer on the negative electrode [19]. The solid electrolyte interphase is formed on the anode surface due to chemical reactions between decomposition products of the electrolyte solvent and lithium salt [20], which in general affects the long-term cell performance. With cycling at high temperatures, the SEI increases its size due to the enhanced decomposition reaction rate of the electrolyte [21]. This leads to an increase in thermal resistance on the anode side due to the thicker additional side reaction layer, which negatively affects the thermal conductivity of the whole system.

Second degradation effect influencing the TC of the cell is closely related to the SEI growth. The evolution of the SEI layer is accompanied by a consumption of the electrolyte, which reduces the degree of wetting of individual battery components. Less electrolyte solvent inside the battery not only reduces the thermal conductivity of the individual layers [6,8], but affects the total TC of the energy storage system [13].

Gas evolution due to electrolyte reduction can also influence the thermal conductivity of a LIB. This effect leads to loss of contact pressure between the internal components, causing overall swelling of the cell packaging [15]. Formed gas bubbles cause local gaps between separator and electrode layers disrupting thermal conduction and thus reducing the thermal conductivity of the whole cell.

In the course of this work, the most significant influence on the thermal conductivity evolution was observed to be the applied compression on the cell during cycling. The effect of charging rate during ageing can be classified as negligible, since little difference was seen in the SOH and TC values for HP and LP aging. Cells, cycled without any compression force acting on the component stack, showed a higher reduction of TC values. Non-compressed cells can experience higher volume changes of the anode active material during intercalation (or extraction) of Li+, leading to a built-up of additional stress and cracking of the graphite [22]. During high-temperature cycling, additional SEI is formed on fractured surface of the anode, which translates into higher amount of electrolyte being depleted. This would decrease thermal conductivity even further, as already seen in the test results, visualised in Figure 2b. In order to reduce cell degradation, a pretension force during cycling is needed. The magnitude of cell compression was observed to have no significant effect on the degradation rate of the investigated batteries.

Thermal runaway prevention of lithium-ion batteries is a critical safety aspect in the automotive industry, which requires particular attention. With increasing product life, the investigated cells experienced a maximum decrease of ~23% in thermal conductivity. TC deterioration shows a reduction also of the critical temperature a cell can safely withstand before entering thermal runaway [23]. The presented results highlight the importance of the adjustment of the cooling system after certain battery lifetime. This would improve heat dissipation for aged cells and reduce the risk of battery overheating, thus increasing battery safety.

4. Materials and Methods

4.1. Samples under Investigation

The cell used in this study is a 41 Ah Li-ion pouch cell with a nominal voltage of 3.7 V, which was obtained by dismounting the battery pack of a commercially available electric vehicle [24]. Regarding the single cell, the electrodes stack consists of 42 polypropylene tri-layer separators, coated with β-Al_2O_3 on the anode side, sandwiched between 21 $LiNiMnCoO_2$-$LiMn_2O_4$ (NMC-LMO) cathodes and 22 graphite anodes. The battery electrolyte, according to the manufacturer, consists of an EC, DEC and PC mixture with $LiPFO_6$.

4.2. Ageing Procedures and Used Equipment

Three different ageing procedures were adopted in this study. The used aging conditions of each are summarised in Table 3.

Table 3. Boundary conditions used during battery cycling.

Ageing Type	Temperature (°C)	C-Rate (C)	SOC Range (%)	Pretension (MPa)
HP	60	1	10–90	0.56
LP	60	3	10–90	0.06
NP	60	1	10–90	0

High temperature during cycling was chosen mainly to achieve fast battery degradation due to the increased reaction rate, which promotes faster growth of the SEI layer due to rapid electrolyte consumption [21]. In order to avoid introducing additional ageing effects inside the batteries by reaching the upper or lower voltage limit during charging/discharging [21] and to shorten the cycling time, a cycling interval between 10–90% SOC was chosen. Different pretension forces were applied to the electrode stack during each ageing procedure. The value during LP cycling was chosen to represent a typical compression that acts upon pouch cells when assembled in a module/pack configuration [25,26]. Even though the applied pretension during the HP-ageing program is too high to be realised in a practical battery pack for automotive applications [26], it can provide a better understanding on how battery properties are affected by an increased external load.

The magnitude of applied compression forces and their even distribution on the battery surface was achieved with a fixture, which comprises of two aluminum plates, positioned on both sides of the battery, tightened by eight M14 bolts. Adjustment of the applied force was realised via plate springs with a well-known deformation characteristic. Four aluminum U-profiles were placed on both sides of the sandwich structure in order to increase the stiffness of the fixture and to prevent the aluminum plates to bend at the edges due to the high amount of pretension force applied. The batteries were mounted between the two aluminum plates and the whole structure was placed inside BasyTec climate chambers with an accuracy of 2 °C in order to be able to control the temperature conditions during cycling. A self-constructed cell-testing unit with a measurement accuracy of 0.2% was utilised for the ageing of batteries under applied high pretension forces, as well as for those with no pretension applied.

End criterion for each ageing strategy was set to 700 cycles in order to ensure comparability of the results. Every 100 cycles the discharge capacity was determined (Figure 3) in order to keep track of the state of health changes with ageing. This was achieved by integrating the charge taken out of battery when discharging the cell from a fully charged state to its lower voltage limit. The capacity loss curves, seen in Figure 3, represent the calculated mean value out of ten individual cells.

In this work, SOH is defined as the ratio of the measured capacities of aged (C_{Aged}) and fresh (C_{Fresh}) batteries, multiplied by 100 to acquire the value in percent. This relationship can be expressed with Equation (1):

$$\text{SOH} = \frac{C_{Aged}}{C_{Fresh}} \times 100 \ (\%) \tag{1}$$

Results of the determined residual capacity after 700 cycles as well as the calculated state of health are shown in Table 4. Similar SOH-values were determined for cells cycled with an applied pretension. For the case of no pretension (NP), stronger cell degradation occurred after cycling, which translated into a higher state of health reduction.
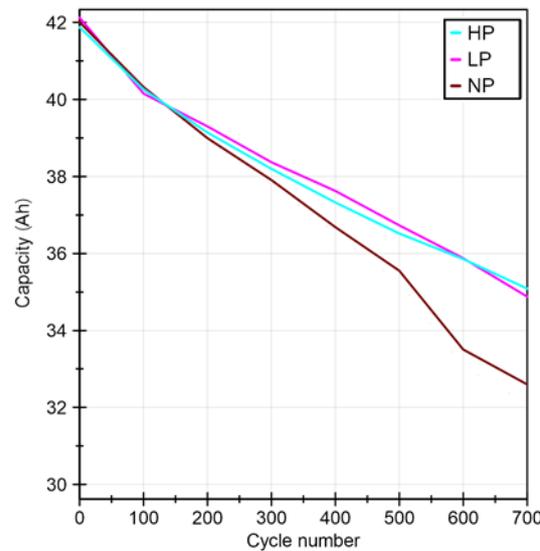
Figure 3. Capacity loss over cycle number for batteries cycled with/without applied pretension.

Table 4. Residual capacity and SOH after ageing.

Cell Description	Residual Capacity (Ah)	SOH (%)
HP	35.1	85.6
LP	34.8	84.9
NP	32.7	79.7

4.3. SOC Setting

Four different SOC levels (0%, 30%, 70%, 100%) were chosen in order to evaluate the change in thermal conductivity of fresh and aged cells over the whole SOC range. The SOC adjustment was performed with a programmable DC power supply (Model number: EA-PSI 9000 3U) an electronic load (Model number: EA-EL 9000 B); a coulomb counter was software implemented thanks to a precision DC Current Transducer (Model number: CT-1000). Fresh and cycle aged batteries were discharged to their lower potential with a 1C discharging rate while maintaining the battery temperature at 20 °C. SOC adjustment was then carried out, starting from 0% SOC, at 1C charging rate, based on the coulomb counting method, which in general relies on the integration of the current supplied to the battery over time. The battery SOC can be expressed using the percentage of capacity that has been charged relative to the current battery capacity (Equation (2)).

$$SOC(t) = SOC(t_0) + \frac{\int_0^t I t dt}{Q_c} \tag{2}$$

Here I (A) denotes the used charging current and Q_c (Ah) is the measured battery capacity.

4.4. Thickness Measurement

Thickness measurements for each battery ageing condition and SOC were conducted using the Platinum 8 ft. model of the FaroArm portable 3D measurement system, having a measurement accuracy of 30 μm according to the manufacturer. The working principle of the device for this application consists of measuring the height difference between the surface where the battery is placed on and the different reference points on the battery. The thickness of fresh and cycle aged cells was determined at 12 evenly distributed points over the whole electrode stack surface and an arithmetic mean value of the thickness was used for the calculation of the thermal conductivity. Since the measurement method requires direct contact with the sample, a metal ruler with known thickness was placed on the battery surface during measurements in order to avoid indentation of the battery pouch

with the measuring tip. The thickness of the ruler was subsequently subtracted from the final calculated value.

A drawback to this method is that it does not take into consideration the topography of the lower battery surface. The assumption that the latter is perfectly flat can result in measuring values with small deviations from actual thickness of the battery at a specific point.

4.5. Measurement Thermal Conductivity

For the determination of the through-plane thermal conductivity, a temperature gradient was forced across the thickness direction of the cell using a temperature guarded plate and a heater until a steady state condition was reached [27]. Temperature values were measured on the top (hot side) and bottom (cold side) of the cell via K-type thermocouples. The heat flux, passing through the sample, is sensed with special flat heat flux sensors with a measurement accuracy of 0.4% as defined by the manufacturer (Hukseflux Thermal Sensors, Delft, The Netherlands). The thermal conductivity—further indicated as k (W/mK)—can be calculated by inserting the measured values into Equation (3). Here F (W/m^2) describes the determined average heat flux, ΔT (K) is the forced temperature gradient and d (m) is the average thickness of the sample.

$$k = \frac{F \times d}{\Delta T} \tag{3}$$

Further details of the used test bench including measurement accuracy can be found in [27].

5. Conclusions

This work highlights the importance of the precise monitoring of the thermal conductivity of Li-ion cells in electric vehicles throughout the entire product life. This can help with the prevention of a premature thermal runaway by making progressive adjustments to the battery cooling system according to the ageing condition. For instance an increased cooling power—as example with higher coolant speed/pressure—could compensate for the altered thermal conductivity and reduce the risk of cell overheating and so increasing battery safety. In the course of this work, an overall decrease of thermal conductivity was measured for cells, aged under different compression forces at high temperatures. This effect was attributed to the combination of the changes to the internal material structure of the electrodes and the depletion of the electrolyte. The degree of degradation of TC was shown to be dependent on the amount of pretension, applied to the component stack of the cell during cycling. Without a compression force, cells experience higher degradation, which translated into a severe reduction of the SOH of the battery and of its thermal conductivity. In order to decrease the deterioration rate of the battery, a good module design and a precise integration of the cell inside a casing that ensures constant pretension of the cells is of great importance.

The generated results can be used as an experimental database for computer simulations to evaluate thermal behaviour of aged lithium ion batteries, in order to predict and prevent thermal runaway propagation. This work can be expanded by determining the multidirectional thermal conductivity of the investigated cell. Future aspects also include measurements on cells, aged under different boundary conditions, as well as comparison of the results of batteries with different chemical composition.

Author Contributions: Conceptualisation, G.K., L.A. and C.E.; methodology, G.K., L.A. and G.G.; investigation, G.K. and A.A.; writing—original draft preparation, G.K. and G.G.; writing—review and editing, L.A., J.H., G.G. and C.E.; review and supervision, W.S.; project administration C.E. All authors have read and agreed to the published version of the manuscript.

Conflicts of Interest: The authors declare no conflict of interest.

Appendix A

Table A1. Data used to calculate the thermal conductivity of fresh cells.

Fresh				
SOC	Thickness	ΔT	Absolute Average Heat Flux	Thermal Conductivity
(%)	(mm)	(°C)	(W/m^2)	(W/mK)
0	7.631	20.450	2002.518	0.747
30	7.691	22.046	2084.933	0.727
70	7.695	21.956	2123.594	0.744
100	7.713	23.857	2407.508	0.778

Table A2. Data used to calculate the thermal conductivity of cells aged under high compression.

HP				
SOC	Thickness	ΔT	Absolute Average Heat Flux	Thermal Conductivity
(%)	(mm)	(°C)	(W/m^2)	(W/mK)
0	7.807	22.851	2113.934	0.722
30	7.861	23.561	2133.937	0.712
70	7.887	25.664	2293.626	0.701
100	7.950	22.233	2150.605	0.770

Table A3. Data used to calculate the thermal conductivity of cells aged under low compression.

LP				
SOC	Thickness	ΔT	Absolute Average Heat Flux	Thermal Conductivity
(%)	(mm)	(°C)	(W/m^2)	(W/mK)
0	8.043	27.487	2439.196	0.714
30	8.092	25.751	2216.222	0.696
70	8.129	28.330	2481.981	0.712
100	8.147	22.984	2164.588	0.768

Table A4. Data used to calculate the thermal conductivity of cells aged without compression.

	NP			
SOC	Thickness	ΔT	Absolute Average Heat Flux	Thermal Conductivity
(%)	(mm)	(°C)	(W/m^2)	(W/mK)
0	8.376	30.735	2116.729	0.578
30	8.500	32.519	2106.614	0.555
70	8.496	32.764	2163.816	0.562
100	8.516	33.696	2548.588	0.645

References

1. Richter, F.; Vie, P.J.S.; Kjelstrup, S.; Burheim, O.S. Measurements of ageing and thermal conductivity in a secondary NMC-hard carbon Li-ion battery and the impact on internal temperature profiles. *Electrochim. Acta* **2017**, *250*, 228–237. [CrossRef]
2. Sheng, L.; Su, L.; Zhang, H. Experimental determination on thermal parameters of prismatic lithium ion battery cells. *Int. J. Heat Mass Transf.* **2019**, *139*, 231–239. [CrossRef]
3. Vertiz, G.; Oyarbide, M.; Macicior, H.; Miguel, O.; Cantero, I.; Fernandez de Arroiabe, P.; Ulacia, I. Thermal characterization of large size lithium-ion pouch cell based on 1d electro-thermal model. *J. Power Sources* **2014**, *272*, 476–484. [CrossRef]
4. Murashko, K.A.; Mityakov, A.V.; Pyrhönen, J.; Mityakov, V.Y.; Sapozhnikov, S.S. Thermal parameters determination of battery cells by local heat flux measurements. *J. Power Sources* **2014**, *271*, 48–54. [CrossRef]
5. Feng, X.; Lu, L.; Ouyang, M.; Li, J.; He, X. A 3D thermal runaway propagation model for a large format lithium ion battery module. *Energy* **2016**, *115*, 194–208. [CrossRef]
6. Burheim, O.S.; Onsrud, M.A.; Pharoah, J.G.; Vullum-Bruer, F.; Vie, P.J.S. Thermal Conductivity, Heat Sources and Temperature Profiles of Li-Ion Batteries. *ECS Trans.* **2014**, *58*, 145–171. [CrossRef]
7. Maleki, H. Thermal Properties of Lithium-Ion Battery and Components. *J. Electrochem. Soc.* **1999**, *146*, 947. [CrossRef]
8. Richter, F.; Kjelstrup, S.; Vie, P.J.S.; Burheim, O.S. Thermal conductivity and internal temperature profiles of Li-ion secondary batteries. *J. Power Sources* **2017**, *359*, 592–600. [CrossRef]
9. Arzberger, A.; Sauer, D.U. The change of thermal conductivity of Lithium-Ion pouch cells with operating point and what this means for battery thermal management. In Proceedings of the AABC—Advanced Automotive Battery Conference, AABTAM Symposium—Advanced Automotive Battery Technology, Application and Market, Atlanta, GA, USA, 2–7 February 2014.
10. Drake, S.J.; Wetz, D.A.; Ostanek, J.K.; Miller, S.P.; Heinzel, J.M.; Jain, A. Measurement of anisotropic thermophysical properties of cylindrical Li-ion cells. *J. Power Sources* **2014**, *252*, 298–304. [CrossRef]
11. Steinhardt, M.; Gillich, E.I.; Stiegler, M.; Jossen, A. Thermal conductivity inside prismatic lithium-ion cells with dependencies on temperature and external compression pressure. *J. Energy Storage* **2020**, *32*, 101680. [CrossRef]
12. Bazinski, S.J.; Wang, X.; Sangeorzan, B.P.; Guessous, L. Measuring and assessing the effective in-plane thermal conductivity of lithium iron phosphate pouch cells. *Energy* **2016**, *114*, 1085–1092. [CrossRef]
13. Bazinski, S.J.; Wang, X. Experimental study on the influence of temperature and state-of-charge on the thermophysical properties of an LFP pouch cell. *J. Power Sources* **2015**, *293*, 283–291. [CrossRef]
14. Maleki, H.; Wang, H.; Porter, W.; Hallmark, J. Li-Ion polymer cells thermal property changes as a function of cycle-life. *J. Power Sources* **2014**, *263*, 223–230. [CrossRef]
15. Mussa, A.S.; Liivat, A.; Marzano, F.; Klett, M.; Philippe, B.; Tengstedt, C.; Lindbergh, G.; Edström, K.; Lindström, R.W.; Svens, P. Fast-charging effects on ageing for energy-optimized automotive LiNi1/3Mn1/3Co1/3O2/graphite prismatic lithium-ion cells. *J. Power Sources* **2019**, *422*, 175–184. [CrossRef]
16. Zhang, Q.; White, R.E. Capacity fade analysis of a lithium ion cell. *J. Power Sources* **2008**, *179*, 793–798. [CrossRef]
17. Fröhlich, K.; Abrahams, I.; Jahn, M. Determining phase transitions of layered oxides via electrochemical and crystallographic analysis. *Sci. Technol. Adv. Mater.* **2020**, *21*, 653–660. [CrossRef]
18. Qian, X.; Gu, X.; Dresselhaus, M.S.; Yang, R. Anisotropic Tuning of Graphite Thermal Conductivity by Lithium Intercalation. *J. Phys. Chem. Lett.* **2016**, *7*, 4744–4750. [CrossRef]
19. Kovachev, G.; Ellersdorfer, C.; Gstrein, G.; Hanzu, I.; Wilkening, H.M.R.; Werling, T.; Schauwecker, F.; Sinz, W. Safety assessment of electrically cycled cells at high temperatures under mechanical crush loads. *eTransportation* **2020**, *6*, 100087. [CrossRef]
20. An, S.J.; Li, J.; Daniel, C.; Mohanty, D.; Nagpure, S.; Wood, D.L. The state of understanding of the lithium-ion-battery graphite solid electrolyte interphase (SEI) and its relationship to formation cycling. *Carbon* **2016**, *105*, 52–76. [CrossRef]
21. Han, X.; Lu, L.; Zheng, Y.; Feng, X.; Li, Z.; Li, J.; Ouyang, M. A review on the key issues of the lithium ion battery degradation among the whole life cycle. *eTransportation* **2019**, *1*, 100005. [CrossRef]
22. Li, P.; Zhao, Y.; Shen, Y.; Bo, S.-H. Fracture behavior in battery materials. *J. Electrochem. Soc.* **2020**, *2*, 22002. [CrossRef]
23. Esho, I.; Shah, K.; Jain, A. Measurements and modeling to determine the critical temperature for preventing thermal runaway in Li-ion cells. *Appl. Therm. Eng.* **2018**, *145*, 287–294. [CrossRef]

24. Kovachev, G.; Schröttner, H.; Gstrein, G.; Aiello, L.; Hanzu, I.; Wilkening, H.M.R.; Foitzik, A.; Wellm, M.; Sinz, W.; Ellersdorfer, C. Analytical Dissection of an Automotive Li-Ion Pouch Cell. *Batteries* **2019**, *5*, 67. [CrossRef]
25. Cannarella, J.; Arnold, C.B. Stress evolution and capacity fade in constrained lithium-ion pouch cells. *J. Power Sources* **2014**, *245*, 745–751. [CrossRef]
26. Barai, A.; Tangirala, R.; Uddin, K.; Chevalier, J.; Guo, Y.; McGordon, A.; Jennings, P. The effect of external compressive loads on the cycle lifetime of lithium-ion pouch cells. *J. Energy Storage* **2017**, *13*, 211–219. [CrossRef]
27. Aiello, L.; Kovachev, G.; Brunnsteiner, B.; Schwab, M.; Gstrein, G.; Sinz, W.; Ellersdorfer, C. In Situ Measurement of Orthotropic Thermal Conductivity on Commercial Pouch Lithium-Ion Batteries with Thermoelectric Device. *Batteries* **2020**, *6*, 10. [CrossRef]